Novel Magnetism and Band Gap Tailoring in N-doped CdS:Cr Nanocomposites for Optomagnetic Applications

SURYA SEKHAR REDDY M[1,2] and KISHORE KUMAR Y B[3]*

[1]Department of Physics, JNTUA, Ananthapuramu, A.P., 515002, India.
[2]Department of Physics, Government Degree College for Women, Madanapalle, A.P., India.
[3]Department of Physics, Mohan Babu University (Erstwhile Sree Vidyanikethan Engineering College), Tirupati, A.P., 517102, India.
*Corresponding author E-mail: msrphd2022@gmail.com

ABSTRACT

Nitrogen and chromium co-doped cadmium sulfide nanocomposites (NCps) were successfully synthesized using a simple co-precipitation method (Cpm). To evaluate their structural attributes, X-ray diffraction (XRD) analysis, conducted with X'pert high score plus software, confirmed the composite nature and established their particle size within the nano range, measuring between 1 to 1.6 nm. Further characterization, employing Fourier transform infrared spectroscopy (FTIR) confirms the presence of Cr and N. The energy dispersive X-ray spectroscopy (EDX) provided compelling evidence of the integration of chromium and nitrogen into the CdS host matrix. An interesting outcome of the UV-VIS diffused reflectance spectra (DRS) analysis was the significant blue shift observed in the band gap resulting from the introduction of chromium, accompanied by a Burstein-Moss effect, leading to a red shift as the nitrogen concentration increased. The intense green light emission witnessed in photoluminescence (PL) studies was associated with the trapping of nitrogen and Cr^{2+} within F-centers. Moreover, vibrating sample magnetometer (VSM) investigations unveiled distinct magnetic behaviors of the nanocomposites, particularly at low magnetic fields. These findings reveal a potential for tailoring band gaps and presenting novel magnetic properties, which could hold substantial promise for applications in optomagnetic and spintronic smart devices.

Keywords: Nanocomposites, Rietveld's analysis, Burstein-Moss effect, Novel magnetism, Spintronics.

INTRODUCTION

In recent years, the scientific community has increasingly turned its attention to cadmium sulfide nanoparticles, which belong to the II-VI semiconductor materials class. These nanoparticles have garnered considerable interest due to their unique size-dependent optical properties, which hold great promise for various applications in optoelectronics[1], telecommunications, data storage[2], and spintronic devices[3]. Among the various methods employed for synthesizing semiconductor nanomaterials, the chemical co-precipitation technique stands out for its simplicity,

cost-effectiveness, and high yield. Notably, it is well-suited for producing well-dispersed, size-controlled particles[4].

In recent progress in this field, researchers have investigated the incorporation of nitrogen into the matrices of various materials, such as ZnO, ZnS, CdS, and graphene/CdS NCps. These innovations have led to significant advancements in the understanding of structural-properties, band gap alterations, magnetic phase transitions, and spin reorientations[5]. Zhou *et al.,* have particularly demonstrated that the alteration of band gap and enhancement of stability of ZnS nanoparticles by inclusion of nitrogen[6]. Similarly, Popov *et al.,* achieved successful nitrogen doping in ZnS through a chemical deposition method[7]. Shi *et al.,* reported the positive impact of nitrogen on stability of graphene/CdS NCps[8].

While the potential applications of chromium-doped CdS nanoparticles in optoelectronics and spintronic devices are promising, research exploring this specific area has been comparatively constrained. The absence of comprehensive research in this domain has inspired the present researchers to investigate CdS and $Cd_{0.96}Cr_{0.04}N_xS_{1-x}$ (x = 0, 2, 4, 6, and 8 at %) nanocomposites as a focal point of their inquiry. Until now, only a limited number of efforts have been undertaken to introduce nitrogen into II-VI nano particles utilizing conventional chemical approaches at lower temperatures. This present study aids in the progression of this evolving field by providing an in-depth analysis of the structural, magnetic, and optical characteristics of CdS and $Cd_{0.96}Cr_{0.04}N_xS_{1-x}$ (x = 0, 2, 4, 6, and 8 at %) NCps, employing 2-mercaptoethanal (ME) as a crucial capping agent. Significantly, to our understanding, this study marks the initial successful attempt in fabricating Cr and N co-doped CdS NCps via the Cpm, utilizing ME as a vital surfactant at room temperature. The investigation provides significant insights into the changes in morphological, structural, magnetic, and optical characteristics induced by this innovative method.

Recent advancements in this field have opened up exciting possibilities for harnessing the distinctive properties of nitrogen-doped and chromium-doped CdS nanomaterials. These advances hold significant potential for the development of next-generation optoelectronic and spintronic devices. As researchers continue to explore and refine the synthesis and characterization of these nanocomposites, we can anticipate further breakthroughs shortly.

Methodology

The nanoparticles CdS and $Cd_{0.96}Cr_{0.04}N_xS_{1-x}$ (x = 0, 2, 4, 6, and 8 at %) were synthesized via the surfactant–assisted Cpm. High-purity Sigma-Aldrich AR grade chemicals, each with a 99.99% purity level, were utilized, obviating the need for further purification. 2-Mercaptoethanol served as the capping agent in the process. The preparation involved the creation of solutions with stoichiometric proportions of 0.2 M $Cd(CH_3COO)_2 \cdot 4H_2O$, $CrCl_3 \cdot 6H_2O$, Na_2S, and CN_2H_4S, all dissolved in de-ionized water. The solutions were thoroughly stirred for 30 minutes. Following this, 2 milliliters of ME, utilized to regulate the grain size, was introduced into the cationic precursor solution of $Cd(CH_3COO)_2 \cdot 4H_2O$. $CrCl_3 \cdot 6H_2O$ and CN_2H_4S were sequentially added dropwise with their proportional volume ratios in a coordinated process. The entire mixture was stirred for an additional 30 minutes. Ultimately, anionic Na_2S was steadily introduced into the solution drop by drop, and the resulting blend was agitated at ambient temperature for duration of 7 h, resulting in the creation of a fine precipitate. The resulting precipitates were separated through filtration and subjected to multiple washes with deionized water to remove impurities. These washed precipitates were then placed in a watch glass and allowed to naturally dry for 48 h within the laboratory environment. Subsequently, the dried material was ground into a fine powder, ensuring uniformity and consistency, before undergoing additional analysis.

The properties related to phase and structures of the synthesized nanoparticles were assessed utilizing a BRUKER D8 advanced powder XRD. Morphological studies were conducted using a Carl FESEM03-81 SEM. Chemical composition studies were carried out using a Carl FESEM03-81 SEM equipped with EDX. Fourier transform infrared spectra were recorded using an Agilent Cavy 360-FTIR instrument with a resolution of 1 cm^{-1} to estimate bond energies. For measurements related to optical properties and energy gap determination, dry powder samples underwent diffuse reflectance measurements utilizing a Perkins Elmer LAMDA 950 UV-VIS-NIR spectrometer. Additionally, room-temperature photoluminescence spectra were recorded using the JY Fluorolog-3-11 spectrometer.

Finally, at room temperature, the magnetic behavior was studied by using a Lakeshore VSM7407.

Structural Analysis

The X-ray diffraction spectra profiles presented in Fig. 1 for both CdS and $Cd_{0.96}Cr_{0.04}N_xS_{1-x}$ (x = 0, 2, 4, 6, and 8 at %) nanoparticles reveal the crystalline structure. Importantly, all XRD patterns correspond to the cubic structure characterized by the space group F-43 m in CdS[9]. The broadening of XRD peaks across all samples is attributed to the remarkably small particle size. The characteristic reflections (311), (220), and (111) found in undoped CdS nanoparticles are consistent with card number C-JCPDS 89e0440, indicating its cubic nature. Moreover, the evident widening of the primary peak in all XRD patterns, specifically at 27°, increases with the addition of chromium dopant, indicating peak broadening. Intriguingly, a pronounced diffraction peak at 48°, indicative of a hexagonal structure (H-JCPDS 77e2306), suggests the presence of hexagonal structural elements in all doped samples. Earlier studies also reported a similar phase change[10], reflecting the dual-phase nature of CdS in the nanocrystalline regime. The similarity between the cubic and hexagonal peaks often results in unresolved phases in the diffraction pattern, particularly with overlapping (220) and (311) reflections. This phenomenon denotes structural changes and the emergence of secondary compounds. The average crystallite size, calculated using the Debye–Scherrer method[11] from the XRD peak widths, falls in the range of 1–1.6 nm. Due to nitrogen's high electronegativity, ionic shifts occur, leading to the formation of unique phases such as Cr_7S_8 and S_2N_4. The resulting structural modifications have been validated through Rietveld's analysis. Peaks broadening underscore the particles' nanocrystalline and composite nature[12].

The observed differences in constituent atom's valency and ionic sizes have led to the development of lattice strain. This strain, as confirmed by the calculated microstrain (ε) using the formula $\varepsilon = \beta/(4 \tan \theta)$, where β = line broadening at FWHM, θ = Bragg's angle, is inversely correlated with increasing dopant concentration. This inverse trend signifies enhanced stability within the composite nanoparticles, resulting in a reduction in crystallite size[13-14]. The structural phase transformations carry significant implications for the electrical and magnetic properties of the as prepared Ncps[3]. The estimated strain and crystallite size values are provided in Table 1.
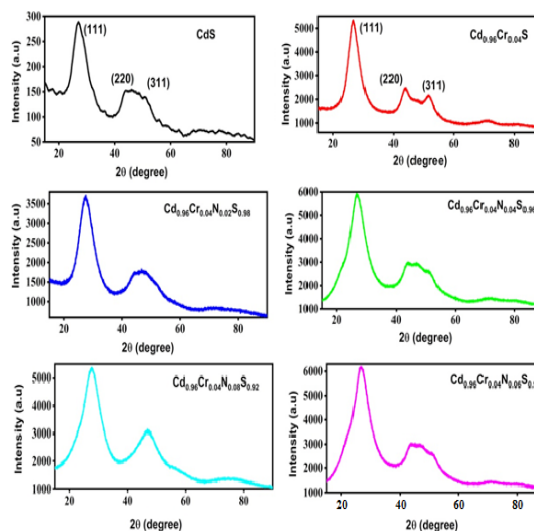

Fig. 1. X-ray diffraction patterns of CdS and $Cd_{0.96}Cr_{0.04}N_xS_{1-x}$ (x = 0, 2, 4, 6, and 8 at %) nanocomposites

Table 1: Crystallite sizes and lattice strains of CdS and $Cd_{0.96}Cr_{0.04}N_xS_{1-x}$ (x = 0, 2, 4, 6, and 8%) nanocomposites

Compound name $Cd_{0.96}Cr_{0.04}N_xS_{1-x}$	Crystallite size (nm)	Lattice strain
CdS	1.08	0.1424
x = 0 %	1.60	0.0971
x = 2 %	1.24	0.1224
x = 4 %	1.09	0.1409
x = 6 %	1.06	0.1479
x = 8 %	1.02	0.1488

SEM with EDX
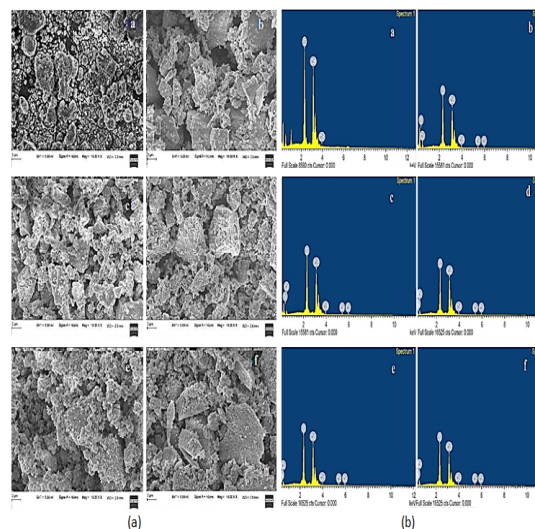
Fig. 2a. FESEM images of CdS and $Cd_{0.96}Cr_{0.04}N_xS_{1-x}$ (x = 0, 2, 4, 6, and 8 at %) NCps
b. EDX analysis of CdS and $Cd_{0.96}Cr_{0.04}N_xS_{1-x}$ (x = 0,2,4,6, and 8 at %) NCps

FESEM offers a valuable means to examine surface morphology, presenting insights into both topographical and cross-sectional views. As depicted in Fig. 2a, the FESEM images of both CdS and $Cd_{0.96}Cr_{0.04}N_xS_{1-x}$(x = 0, 2, 4, 6, and 8 at %) NCps are presented. Notably, the morphology of CdS Nps reveals a distribution of non-uniformly sized loosely packed grains. However, as the concentration of nitrogen in $Cd_{0.96}Cr_{0.04}N_xS_{1-x}$ (x = 0, 2, 4, 6, 8, and 8 at %) NCps increases, a noticeable decrease in the size of closely arranged grains becomes evident. The decrease in grain size can be associated with grain boundary reconfiguration, resulting in an increase in lattice strain[15]. The development of lattice strain and changes in grain domain sizes occur due to adjusted lattice parameters, causing internal stress within the material. The resultant internal stress, consequently, impedes the grains' development, accounting for the smaller grain sizes observed in $Cd_{0.96}Cr_{0.04}N_xS_{1-x}$ (x = 0, 2, 4, 6, and 8 at %) NCps compared to CdS nanoparticles.

In Fig. 3b, the energy dispersive X-ray spectroscopy analysis of both CdS and $Cd_{0.96}Cr_{0.04}N_xS_{1-x}$ (x = 0, 2, 4, 6, and 8 at %) NCps is presented. These profiles provide concrete evidence of the presence of elements such as chromium, cadmium, and sulfur. Furthermore, the incorporation of nitrogen into the lattice of $Cd_{0.96}Cr_{0.04}N_xS_{1-x}$ (x = 0, 2, 4, 6, and 8 at %) NCps is confirmed through EDX analysis, shedding light on the elemental composition of these nanocomposites.

Optical Studies
### FTIR studies

In Fig. 3, the Fourier transform infrared spectra of both CdS and $Cd_{0.96}Cr_{0.04}N_xS_{1-x}$ (x = 0, 2, 4, 6, and 8 at %) NCps are displayed. A distinct peak at 3282 cm^{-1}, attributed to the stretching vibration of -OH, $-NH_2$, and $-CONH_2$ groups, highlights the robust interaction between these functional groups and CdS[8]. Significantly, the widening and movement of this peak towards shorter wavelengths indicate the effective inclusion of N and Cr within the CdS structure[16]. The bending corresponding to C=C bending, C=C stretching, and N–H was observed at 1548 cm^{-1}, 1403 cm^{-1}, and 1646 cm^{-1} in additional peaks[17]. The 1001 cm^{-1} peak is associated with C-O stretching, and the 1050 cm^{-1} peak is the outcome of C-N bond stretching[17]. These results confirm the use of ME as a surfactant for controlling the size of the nanocomposites.
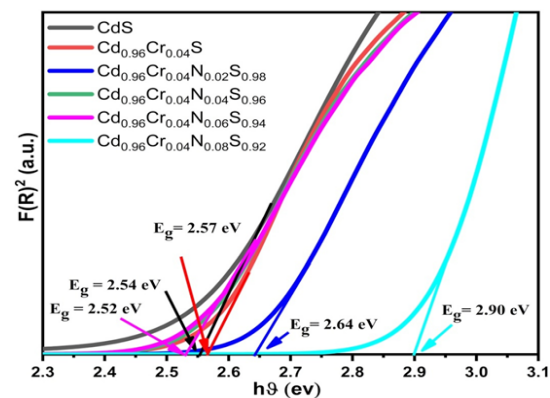
Table 2: Band gap values of CdS and $Cd_{0.96}Cr_{0.04}N_xS_{1-x}$ (x = 0, 2, 4, 6, and 8 at %) NCps

Compound $Cd_{0.96}Cr_{0.04}N_xS_{1-x}$	Band gap(eV)
CdS	2.54
x = 0 %	2.64
x = 2 %	2.52
x = 4 %	2.53
x = 6 %	2.57
x = 8 %	2.90
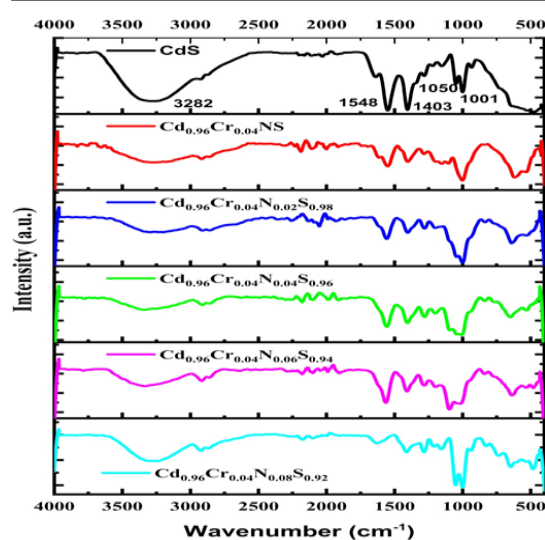
Fig. 3. FTIR spectra of CdS and $Cd_{0.96}Cr_{0.04}N_xS_{1-x}$ (x = 0, 2, 4, 6, and 8 at %) NCps

UV-VIS DRS spectra

Fig. 4. Kubelka-Munk plots of CdS and $Cd_{0.96}Cr_{0.04}N_xS_{1-x}$ (x = 0, 2, 4, 6, and 8 at %) NCps

For assessing the samples' band gaps, Kubelka-Munk plots were produced from the DRS,

showcased in Fig. 4, illustrating both CdS and $Cd_{0.96}Cr_{0.04}N_xS_{1-x}$ (x = 0, 2, 4, 6, and 8 at %) NCps. The determined band gap values are detailed in Table 2. The initial band gap value for the as-prepared CdS nanoparticles measures 2.54 eV, surpassing the bulk CdS band gap of 2.42 eV[18]. This deviation signifies the presence of a quantum confinement effect. With the incorporation of chromium, the band gap value ascends from 2.54 eV to 2.64 eV, subsequently decreasing to 2.52 eV with the addition of nitrogen, a phenomenon attributed to the Burstein-Moss effect[9]. An observable pronounced shift to a blue band gap is witnessed with a rising nitrogen concentration, reaching 2.90 eV. This change is attributed to the interaction between the band electrons in CdS and the localized d electrons of the dopant ions, known as d-d exchange[10].

The upward shift to higher energy levels, referred to as the blue shift, is a direct consequence of the diminutive particle size, brought about by the quantum confinement effect. These findings underscore the potential for band gap tailoring through nitrogen doping in CdS:Cr, exemplified by the substantial enhancement of band gaps ranging between 2.52 eV to 2.90 eV, representing a noteworthy variation of 0.48 eV. These outcomes hold practical implications in the domains of optoelectronics, optomagnetics, and spintronics devices.

PL studies

Figure 5 illustrates the room temperature photoluminescence spectra of both CdS and $Cd_{0.96}Cr_{0.04}N_xS_{1-x}$ (x = 2,4,6, and 8 at %) NCps. In CdS, a noticeable blue emission band appears at 512 nm. This is accompanied by two extra peaks observed at 440 nm and 416 nm. This specific emission at the band edge arises from the recombination of excitons or electron-hole pairs that are shallowly trapped[10].

With the introduction of nitrogen and chromium dopant ions, a noteworthy reduction in luminescence intensity, on the order of magnitude, is observed. Upon closer inspection, it's evident that CdS doped with N and Cr displays a broad and strong emission band ranging from 450 nm to 620 nm, with its maximum intensity situated at 520 nm. This is accompanied by a violet emission shoulder at 467 nm near the band edge, which arises from transitions between surface states and the valence band. The broadened emission peak may be credited to the merging of emissions originating from diverse defects formed during Cr and N doping within the CdS structure. Furthermore, a weak emission near the band edge peak is detected at 750 nm, associated with the presence of sulfur vacancies referred to as F-centers.

Notably, as dopant concentrations increase, a reduction in luminescence intensity is observed, which may be attributed to non-radiative recombination processes involving numerous excited electrons and holes[19]. This phenomenon, known as dopant-induced quenching, is a common occurrence in nanoparticles and has been previously reported in the case of Cr-doped ZnS and CdS. The observed shifts in photoluminescence emission peaks are ascribed to variations in the position of defects within the band gap. The potential of nitrogen-doped CdS:Cr nanoparticles in future white light-emitting devices.
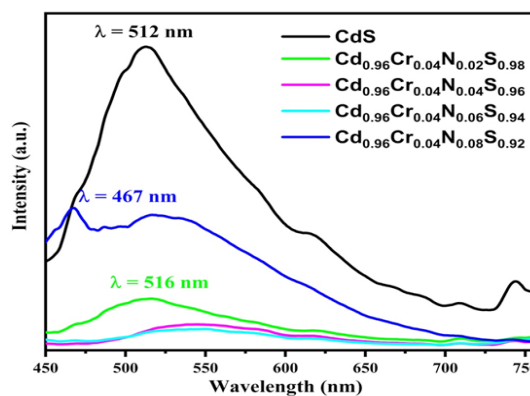

Fig. 5. PL spectra of CdS and $Cd_{0.96}Cr_{0.04}N_xS_{1-x}$ (x = 2, 4, 6, and 8 at %) NCps

VSM studies

In Fig. 6, the M-H curves of CdS and $Cd_{0.96}Cr_{0.04}N_xS_{1-x}$ (x = 0, 2, 4, 6, and 8 at %) NCps reveal room-temperature ferromagnetism (RTFM). The magnetic susceptibility is fascinating as it consists of both ferromagnetic and diamagnetic components. The ferromagnetic background is superimposed onto the diamagnetic loop[3]. The ferromagnetic response was plotted in the inset of Fig. 6 after deducting the dia magnetic contribution. The distinct S-shaped open curves in this ferromagnetic response confirm the presence of room-temperature ferromagnetic properties in $Cd_{0.96}Cr_{0.04}N_xS_{1-x}$ (x = 0, 2, 4, 6, and 8 at %) NCps, particularly in the presence of low magnetic fields

(less than 3 KOe)[20]. This ferromagnetism is attributed to localized defects within the crystal structure, interactions between secondary compounds formed by doping elements, and the inherent nature of the carrier medium.

The investigation of synthesis conditions and the observed properties requires a detailed analysis to determine the origin of this ferromagnetism. Prior research by Madhu *et al.,* Mondal *et al.,* and Yang *et al.,* suggested various explanations for magnetism, such as surface states and sulfur vacancies[9,21]. However, in the present investigation, neither sulfur vacancies nor cadmium vacancies appear to account for the observed ferromagnetism. Photoluminescence studies suggest that increased N and Cr dopant concentrations lead to enhanced defect formation, while magnetic assessments suggest that higher levels of dopants result in the reduction of magnetic characteristics. Additionally, the apparent ferromagnetic characteristics are not associated with the generation of metallic clusters or precipitates within the manufactured samples. These formed specimens contain acknowledged antiferromagnetic phases, like Cr_7S_8 and S_2N_4, which were excluded through Rietveld's analysis of all XRD patterns. Therefore, it is suggested that the observed magnetic traits in this materials are linked to Cr substitution within the CdS lattice, aligning with findings reported by Elavarthi *et al.,*[10].
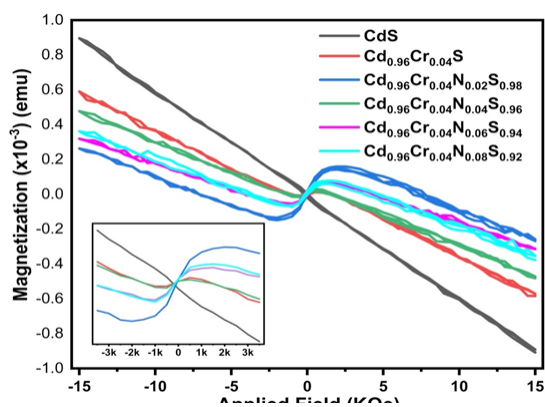

Fig. 6. VSM spectra of CdS and $Cd_{0.96}Cr_{0.04}N_xS_{1-x}$ (x = 0, 2, 4, 6, and 8 at %) NCps

The swift reduction in effective saturation magnetization (M_s) per chromium atom as nitrogen content increases might be due to deteriorating crystal quality or intensified antiferromagnetic interaction at elevated nitrogen concentrations. Consequently, the room-temperature ferromagnetic

values at low fields are associated with local defects, interactions between anti-ferro magnetic secondary compounds, and the presence of Cr metallic ions in the synthesized nanoparticles[22]. As the applied magnetic field increases, the antiferromagnetic interactions eventually suppress the ferromagnetism. This novel magnetic behavior has significant potential for applications in optomagnetic, optoelectric, and spintronic smart devices.

CONCLUSION

The synthesis and thorough characterization of nitrogen and chromium co-doped cadmium sulfide nanocomposites through a surfactant-assisted chemical co-precipitation method have revealed intriguing properties and potential applications. The XRD demonstrated the presence of multiple phases in these nanocomposites and established their particle size in the nano range, offering a foundation for further investigation. FTIR, FESEM with EDX provided concrete evidence of the successful incorporation of chromium and nitrogen into the cadmium sulfide host matrix.

Notably, the UV-VIS diffused reflectance spectra analysis unveiled a significant blue shift in the band gap, accompanied by a Burstein-Moss effect leading to a red shift as the nitrogen concentration increased. This effect has the potential to open new avenues for applications in optomagnetic and spintronic smart devices. Additionally, the strong green light seen in photoluminescence tests was linked to nitrogen and Cr^{2+} ions being captured in F- centers, adding another dimension to the unique optical properties of these nanocomposites. Lastly, vibrating sample magnetometer investigations unveiled novel magnetic behaviors at low magnetic fields, further expanding the potential applications of these materials. In conclusion, the tailoring of band gaps and the emergence of novel magnetic properties make these NCps a promising candidate for various optomagnetic and spintronic applications, ushering in the prospect of innovative smart devices in the field.

art analytical instruments were instrumental in our research endeavors.

Conflict of interest

The authors declare no potential conflicts of interest in this research. This work was conducted without any financial or personal relationships that could inappropriately influence or bias the content or interpretation of the study.

REFERENCES

1. Moghaddam, M.; Naderi, N.; Hosseinifard, M.; Kazemzadeh, A. *Ceram. Int.*, **2020**, *46*, 7388–7395.

2. Kumar, K. S.; Divya, A.; Reddy, P. S. *Appl. Surf. Sci.*, **2011**, *257*, 9515–9518.

3. Nabi, A.; Akhtar, Z.; Iqbal, T.; Ali, A.; Javid, M. A. *J. Semicond.*, **2017**.

4. Prabhu, R. R.; Abdul Khadar, M. *Pramana-J. Phys.*, **2005**, *65*, 801–807.

5. Kaur, M.; Kumar, V.; Singh, J.; Datt, J.; Sharma, R. *Mater. Technol.*, **2022**, *37*, 2644–2658.

6. Zhou, Y.; Chen, G.; Yu, Y.; Yujie Zheng, Y.; He, F.; Han, Z. *Phys. Chem. Chem. Phys.*, **2015**, *17*, 1870–1876.

7. Popov, I. S.; Kozhevnikova, N. S.; Melkozerova, M. A.; Vorokh, A. S.; Enyashin, A. N. *Mater. Chem. Phys.*, **2018**, *215*, 176–182.

8. Shi, W.; Guo, F.; Li, M.; Shi, Y.; Tang, Y. *Sep. Purif. Technol.*, **2019**, *212*, 142–149.

9. Madhu, C.; Sundaresan, A.; Rao, C. N. R. *Phys. Rev. B-Condens. Matter Mater. Phys.*, **2008**, *77*, 3–6.

10. Elavarthi, P.; Kumar, A. A.; Murali, G.; Reddy, D. A.; Gunasekhar, K. R. *J. Alloys Compd.,* **2016**, *656*, 510–517.

11. Gadalla, A.; Almokhtar, M.; Abouelkhir, A. N. *Chalcogenide Lett.*, **2018**, *15*, 207–218.

12. Poornaprakash, B.; Subramanyam, K.; Cheruku, R.; Kim, Y. L.; Pratap Reddy, M. S.; Minnam Reddy, V. R. *Mater. Sci. Semicond. Process.*, **2021**, *134*, 106055.

13. Pandey, G.; Dixit, S.; Shrivastava, A. K. *Mater. Sci. Eng. B Solid-State Mater. Adv. Technol.*, **2015**, *200*, 59–66.

14. Saikia, D.; Jami, J.; Borah, J. P. Phys. B *Condens. Matter.*, **2019**, *565*, 25–32.

15. Kumar, S.; Sharma, J. K. *Mater. Sci. Pol.,* **2016**, *34*, 368–373.

16. Reddy, D. A.; Liu, C.; Vijayalakshmi, R. P.; Reddy, B. K. *Ceram. Int.*, **2014**, *40*, 1279–1288.

17. Chand, P.; Ghosh, R.; Sukriti. *Optik (Stuttg).,* **2018**, *161*, 44–53.

18. Muruganandam, S.; Anbalagan, G.; Murugadoss, G. *Optik (Stuttg).,* **2017**, *131*, 826–837.

19. Giribabu, G.; Murali, G.; Reddy, D. A.; Liu, C.; Vijayalakshmi, R. P. *J. Alloys Compd.*, **2013**, *581*, 363–368.

20. Reddy, M. S. S.; Vandana, C. S.; Kumar, Y. B. K. *Indian J. Sci. Technol.*, **2023**, *16*, 2024–2034.

21. Zhang, Z.; Han, L.; Xie, G.; Liao, Q.; Zhong, B.; Yu, Y. *J. Mater. Sci. Mater. Electron.,* **2016**, *27*, 12940–12946.

22. Mandai, S. K.; Nath, T. K.; Das, A. K.; Karmakar, D. *J. Appl. Phys.*, **2007**, *101*.